MODELING AND OPTIMIZATION OF DIRECTIVE ACOUSTICAL PARTICLE VELOCITY SENSORS FOR ULTRASONIC APPLICATIONS

L. Benvenuti[a], A. Catania[a], P. Bruschi[a,b], M. Piotto[a,b]

[a]Dipartimento di Ingegneria dell'Informazione, University of Pisa, via G. Caruso 16, I-56122 Pisa, Italy

[b]IEIIT-Pisa, CNR, via G. Caruso 16, I-56122, Pisa, Italy

Abstract

Acoustical particle velocity sensors for applications in the ultrasonic frequency range are investigated by means of finite element simulations. The operating principle of these devices is modulation of the heat transfer between pairs of parallel microwires, caused by the propagation of the acoustic wave. The sensing structure has been designed to be compatible with a commercial CMOS process followed by a simple post-processing procedure. An efficient enhanced-2D model has been used for the simulation of three different sensing structures. The dependence of the frequency response on geometrical parameters is investigated, demonstrating that one of the three analyzed structures can be actually optimized to obtain usable performances up to ultrasound frequencies.

Keywords: Acoustic particle velocity sensor; CMOS-compatible; FEM simulations; Ultrasound applications.

Corresponding Author:
Massimo Piotto,
Dipartimento di Ingegneria dell'Informazione,
University of Pisa,
via G. Caruso 16,
I-56122, Pisa, Italy
Tel +39 050 2217657,
Fax +39 050 2217522,
e-mail: massimo.piotto@unipi.it

1. Introduction

The propagation of a sound wave in a medium is characterized by a scalar quantity, the pressure, and a vector quantity, the acoustic particle velocity (APV) [1]. The knowledge of both quantities allows a complete description of the acoustic field and direct determination of the acoustic impedance and the acoustic intensity. Pressure measurement is performed by means of standard microphones, while the detection of the APV is usually more complicated and different solutions have been proposed so far. Direct measurement of the particle velocity is quite simple in water [2], while in air the particle velocity has been traditionally inferred from gradient pressure measurements because reliable direct methods were based on cumbersome and expensive optical devices [3]. In 1995, de Bree *et al.* proposed for the first time a micromachined thermal sensor, named μ-Flown, capable of a direct detection of the APV in air [4, 5]. The device consists of a pair of parallel heated platinum microwires integrated on suspend dielectric beams; its operation is based on the heat transfer between the wires caused by the propagation of the acoustic wave. Asymmetrical heat transfer turns into temperature variations that are detected through the temperature dependence of the wire resistance. These sensors are sensitive to a single component of the APV vector (along the axis perpendicular to two wires). Since the latter is parallel to the propagation direction in far field conditions (plane or spherical waves), APV sensors are intrinsically directive [6]. The device has been progressively improved increasing the sensitivity, leading to the introduction of commercial acoustic probes based on this type of APV sensor [7]. Similar devices, consisting of multiple pairs of heated wires, integrated on the same chip by means of dedicated micromachining technologies, have been proposed for 2D [8-10] and 3D [11-13] APV measurements. Recently, the possibility of fabricating APV sensors with a CMOS-compatible fabrication technique has been demonstrated [14-16]. APV sensors have been proposed for diverse applications, including acoustic impedance and absorption coefficient measurement [17-19], sound intensity measurement [20], direction of arrival estimation [21], near-field acoustic holography [22,23]

and noise source localization [24]. A field in which the possibility of using APV sensors has not yet been explored is that of ultrasounds. In addition to the well-known use in medicine, ultrasounds find application in various fields, including structure health monitoring [25, 26], quality control of food [27], rangefinders and obstacle detection [28-30]. In particular, ultrasound sensors working at 40 kHz have been largely used for obstacle detection in the safe navigation of robots [28, 29], autonomous vehicles [30-32] and in the navigation aid of visually impaired or blind persons [33-35]. Ultrasonic sensors based on vibrating membranes are widely used because they are cheap and have a low power consumption. However, they have a poor angular resolution since they cannot usually identify the angular location of the obstacle inside a cone with an aperture of about 60 degrees. For this reason, applications requiring not only the object detection but also its precise localization implement complex strategies based on array of sensors [33], rotating sonar [30] or data fusion from different typologies of transducers [34, 35]. In these applications, an ultrasonic transducer with a high directivity would be very useful to reduce the complexity of the sensor system. The APV sensors could be a good candidate because they are intrinsically directive with the maximum/minimum sensitivity axes that can be electronically tuned by using only two orthogonal elements [36].

In this work, we investigate for the first time the possibility of extending the use of the APV sensor to the ultrasonic frequency range. The high frequency limit is determined by the thermal capacitance of the sensing structures [37], which depends on the volume of the wires and their supporting elements. For this reason, we have studied three sensing structure typologies with different wire volumes. In particular, the sensing structures consist in pairs of parallel polysilicon-silicide wires placed on silicon dioxide membranes suspended on a cavity etched into the silicon substrate. The APV sensor has been designed to be compatible with a fabrication flow consisting of a commercial CMOS process followed by a simple post-processing step, necessary to suspend the wires. For the parameters of the CMOS process, reference to a real technology of STMicroelectronics has been made. The geometric dimensions of each structure have been optimized in order to obtain the maximum sensitivity. The

optimization has been performed by means of finite element simulations based on an original enhanced 2D model [15], whose greater computational efficiency, with respect to full 3D models, allowed the execution of detailed parametric sweeps in reasonable times.

2. Device description

The sensing structure is similar to that proposed in our previous works [14-16] and only a brief description is reported here. The device consists of two polysilicon-silicide resistors immersed in the fluid (air) where the acoustic wave propagates. The resistors are heated up to a few hundred Kelvins above the fluid temperature by an electric current. The resistors are thermally insulated from the silicon substrate by integrating them into suspended silicon dioxide membranes. In particular, each wire has been divided into short segments placed on its own U-shaped membrane, as schematically shown in Fig. 1 for the case of a three-segment wire pair.

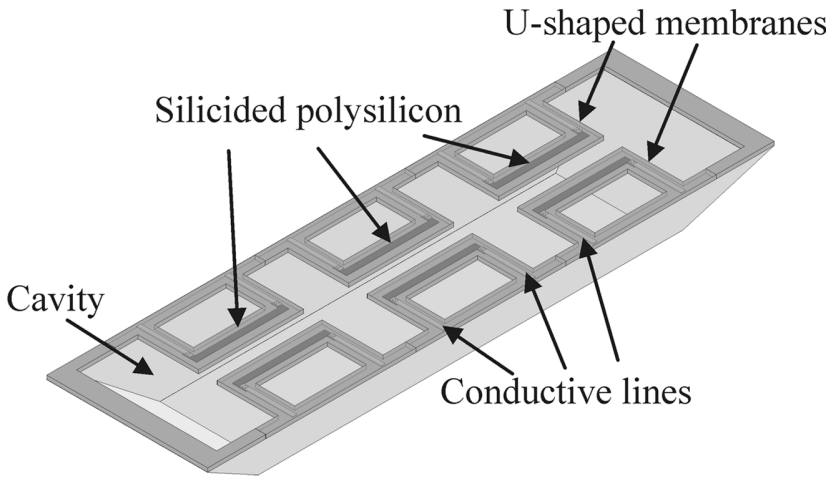

Fig. 1. Schematic perspective view of a sensing structure. (not to scale)

The segments consist of polysilicon-silicide lines, which are polysilicon interconnects that are processed to form a superficial thin layer of a metal-silicon compound (silicide). In commercial CMOS processes, the aim of this process is to reduce the sheet resistance of the interconnections. In the case of APS sensors, use of polysilicon-silicide instead of polysilicon allows for a higher temperature coefficient (higher sensitivity). The segments are placed on the longest side of the U-shaped

membranes while the other two sides of the membranes support the conductor lines necessary to connect the segments together to form the wire. The cavity, that separates the membranes from the substrate, has been fabricated by applying a post-processing technique where the silicon anisotropic etching is performed after the conclusion of the standard CMOS fabrication process. Partitioning of the long wire into shorter section allows for smaller U-shaped membranes and this has two positive effects. First, smaller membranes have a better mechanical robustness and this increases the reliability of the device. Second, U-shaped membranes of small dimensions can be suspended using silicon etching times short enough to be applicable as a post-processing step to chip fabricated with a standard CMOS process. TMAH solutions are usually used for the silicon etching because they show a very good selectivity towards the dielectric layers that separates the interconnect layers and protect the chip surface. In this way, it is possible to perform the substrate etching using the standard dielectric layers of the process as a mask. Therefore, post-processing requires only a single photolithography step to define this dielectric (silicon dioxide) mask. Opening of the dielectrics down to the silicon substrates is conveniently performed by means of Reactive Ion Etching (RIE). Unfortunately, the bonding pads (aluminum) should be already free of the protecting dielectric layer when the TMAH substrate etching is applied, since no further photolithography can be applied after release of the membranes. Although TMAH etches aluminum at a much slower rate than silicon, particularly long etching times results in damage of the bonding pads. This aspect limits the maximum TMAH etching times.

The devices proposed in this work have been designed taking into consideration the properties (layer thicknesses, material properties, design rules) of a commercial CMOS process of STMicroelectronics. Fig. 2 shows a perspective and a plan view of a U-shaped membrane with the main dimensions indicated. APS sensors fabricated with processes described so far showed a sensitivity that rapidly drops over a few kHz [15,37], being de facto not applicable for ultrasound applications. In this work, we have investigated the possibility to extend the frequency bandwidth of these structures by changing the geometry with respect to the previously proposed devices.

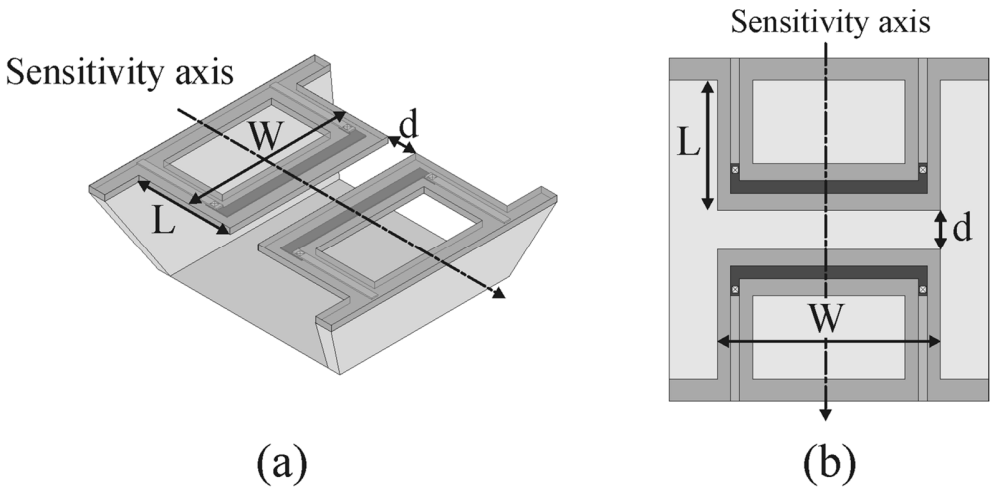

Fig. 2. (a) Perspective and (b) plan view of a section of the sensing structure. The axis of maximum sensitivity is shown. (not to scale)

Not all the dimensions can be changed freely because some of them affect diverse aspects of the sensor behaviour. For example, the selection of the length (L) and the width (W) of the suspended membrane have to take into account both the required thermal insulation and the structure feasibility. In fact, high values of L and W guarantee a very good thermal insulation and then improved sensitivity at all frequencies, but turn out into long etching times and low mechanical robustness. As a trade-off, we have chosen L=41 μm and W=59 μm. Conversely, other dimensions, like the width of the polysilicon-silicide lines, metal lines and dielectric arms, must be reduced as much as possible to reduce heat loss and thermal capacitances. Fabrication issues (mainly due to the process design rules) practically dictated the values used in this work. Instead, the wire distance (*d*) is a parameter that can be modified without impact on the fabrication process. However, it affects the sensor performances in a way that it is not possible to determine with intuitive arguments [37]. Therefore, the wire distance has not been fixed in the simulations but extensive parametric sweeps have been performed to characterize the effects of this quantity, with particular emphasis on the optimization of the sensitivity to ultrasounds. In addition, the membrane thickness is a parameter that can be easily modified during the post-processing by slightly changing the sensor design and/or post-processing sequence. This parameter affects the thermal capacitance associated to the membrane mass, which is the main limitation to the possibility of

detecting high frequency signals. Therefore, we investigated the possibility of reducing the membrane mass preserving the feasibility of the sensing structure. To this aim, three distinct configurations have been designed, differing mainly for the thickness of the silicon dioxide membrane, as schematically shown in Fig. 3.

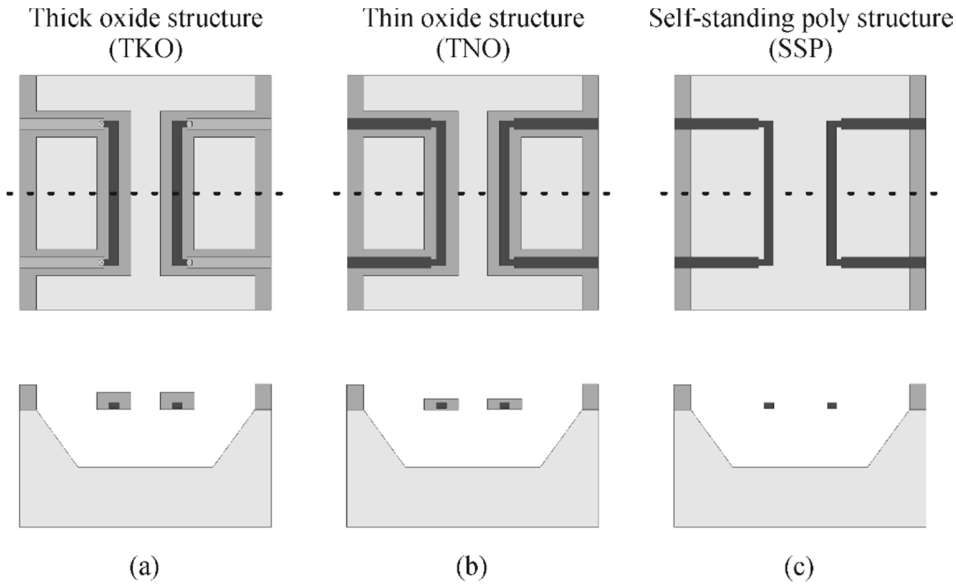

Fig. 3. Plan and cross-section views of the three different sensing structures (not to scale): (a) thick oxide structure (TKO), (b) thin oxide structure (TNO) and (c) self-standing polysilicon structure (SSP).

In the structure shown in Fig. 3a, definition of the silicon dioxide membranes exploits the second metal layer (metal 2) as a mask during the RIE etching in the post-processing. This strategy, proposed in [14, 15] for acoustic sensors and in [38] for thermal flow sensors, allows reducing the silicon dioxide thickness over the membranes to about 50 % of the whole dielectric stack of the process in a very simple and controlled way. Furthermore, definition of the metal 2 mask geometry occurs during the execution of the CMOS process and, for this reason, is marked by the typically high resolution and alignment accuracy of modern microelectronic technologies. Only an additional low-resolution photoresist mask is required to broadly select the sensor areas. This photoresist layer is also exploited to allow removal of the metal-2 mask over the membrane without affecting the bonding pads. As a consequence, the resolution/alignment specifications of the final post-processing steps are significantly

relaxed, making it affordable for research lab or small-medium enterprises. In this first structure (Fig.3a), indicated with thick oxide structure (TKO) for the relatively high residual thickness of the membranes, the conductor lines, necessary to connect the segments together to form the wire, are made of the first metal layer (metal1, aluminum). This choice keeps joule heating along the short sides of the membrane to a minimum, but degrades thermal insulation of the wires, due to the high thermal conductivity of aluminum.

An evolution of the proposed definition strategy can be obtained using the metal-1 layer (instead of metal2) as the RIE mask to fabricate the structure shown in Fig. 3b. In this case, the dioxide thickness is decreased by 75 % with respect to the total amount of the dielectric layers and for this reason we named this structure thin oxide structure (TNO). Obviously, with this choice, the metal-1 layer is no more available for interconnections. The proposed solution is to use polysilicon-silicide lines with increased width across the connection arms to reduce Joule heating along the latter (wasted power).

The last evolution of the process consists in the removal of the thin silicon dioxide membrane after the silicon anisotropic etching, obtaining a self-standing polysilicon-silicide wire as schematically shown in Fig. 3c. Removal of the supporting membrane can be obtained with a time-calibrated etching of the silicon dioxide using a HF based solution. With this structure, named self-standing polysilicon structure (SSP), the minimum thermal capacitance is achieved for the wire. The width of the supporting polysilicon arms (perpendicular to the wire) is increased to reduce unproductive Joule heating (as for the structure in Fig.3b) and to guarantee good mechanical robustness.

As mentioned earlier, the design of the structures requires the optimization of many geometrical parameters and, in some cases, a trade-off between different requirements should be taken into account. The proposed sensor is a complex continuous system with the interaction of different physical mechanisms that cannot be represented by means of an accurate analytical model. For this reason, the design and optimization of the sensing structures have been performed with the FEM model described in the next section.

3. FEM model

The FEM model of the sensing structures has been developed using the COMSOL Multiphysics platform. The model relies on a multilevel approach that was originally proposed in [15] and validated through comparison with experimental data. Briefly, the static solution obtained with a 3D model is used to tune the dynamic 2D model, which is actually employed to obtain the sensor response to acoustic waves. In Fig. 4 an axonometric projection of the geometric structure used in the 3D model is shown. It can be noted that only half of the structure shown in Fig. 2a has been simulated, taking advantage of the symmetry of the structure about the x-z plane.

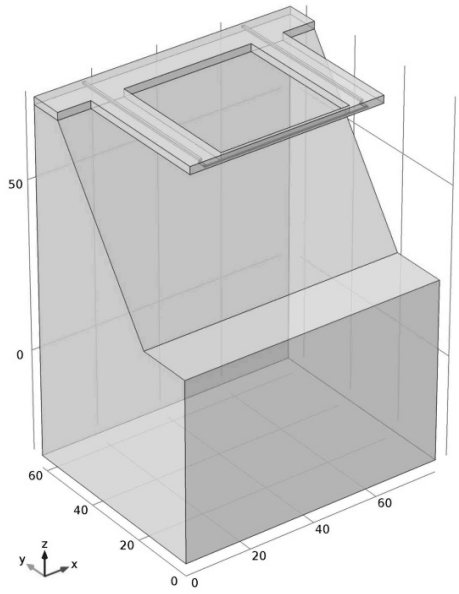

Fig. 4. Axonometric projection of the 3D COMSOL model used for the FEM numerical simulations

The 3D model has been used to simulate only the static power dissipation of the sensing structure immersed in still air. In fact, the solution of the complex thermo-acoustic phenomena in a large 3D model has proven to be unpractical, since very long simulation times are required, especially for the parametric sweeps that are necessary to optimize the structure design. Furthermore, memory limits impose the reduction of the mesh complexity, impairing the solution accuracy. On the other hand, a simple 2D model based on a y-z section of the structure is far from being adequate, since it completely

ignores heat transfer along the x-axis, resulting in hugely overestimated thermal insulation. For this reason, we decided to develop an efficient 2D model where heat loss along the x-axis of the structure is taken into account with proper additional terms. This simulation approach can be considered an enhanced 2D model, which was demonstrated to be capable of predicting the experimental characteristics of thermal flow sensors [39] and acoustic particle velocity sensors [15]. In practice, the 2D model has been modified so that the considered y-z section of the wire approximates the same thermal characteristics of the full wire simulated with a 3D model and averaged along the x-axis.
In particular, the simulation procedure can be divided into the following four steps.

-) *3D Model – stationary simulation*: the first step is the stationary simulation of the structure using the electro-thermal modules in order to calculate the temperature distribution as a function of the voltage applied across the wire. The average values of the temperature (T_{avg}) and power dissipation (P_{avg}) of the polysilicon wire are calculated.

-) *2D Model – stationary simulation*: the second step is the stationary simulation of the 2D Model using the heat transfer module. The mean power dissipation value (P_{avg}) calculated at the previous step is applied as heat source boundary conditions at the wire section; the heat losses to the substrate through the membrane along the x-axis are considered as an out-of-plane heat flux boundary condition applied at the same wire section. The out-of-plane heat flux is a boundary condition available for 2D models that specifies an amount of heat flux in the direction perpendicular to the plane of the model by means of the following formula:

$$q = h(T_{ext} - T) \tag{1}$$

where q is the heat flux, h is the heat transfer coefficient, T_{ext} is the external reference temperature and T is the temperature of the boundary. In our model, the value of h has been trimmed in order to obtain a mean static temperature of the polysilicon wire equal to that calculated with the 3D Model at the previous step (T_{avg}). In this way, the stationary 2D Model results to be equivalent to the 3D Model in terms of average values. It is important to note that the heat losses introduced with the out-of-plane

boundary condition are not constant, but they depend on the temperature (T) of the wire section. This condition is consistent with the real behavior of the heat losses through the membrane and it is fundamental in order to obtain accurate results in the following dynamic simulations where the wire temperature varies due to the acoustic wave.

-) *2D Model – frequency domain simulation*: the third step is the acoustic simulation in the frequency domain with the thermo-acoustics module. This module includes the viscous losses and the thermal conduction effects near walls that cannot be neglected when acoustic waves interact with small geometries as in our device. A constant particle velocity is applied to one side of the air volume, while an acoustic impedance boundary condition is used at the other extreme of the air volume. The static temperature distribution calculated in the previous step is used as input equilibrium temperature. The output of this step is the particle velocity distribution expressed in terms of a complex time dependent field; the actual value at any point in time is the real part of the solution.

-) *2D Model –time dependent simulation:* the last step is the time-dependent thermal simulation with the heat transfer module. The initial temperature distribution is the stationary solution previously calculated. The convective heat transfer caused by the acoustic wave is taken into account by imposing a sinusoidal air velocity field as model input. The phase and the magnitude of the velocity distribution are those calculated by means of the acoustic module in the previous step. After a short transient, a steady state solution is reached where the temperatures of the two wires oscillate in a sinusoidal fashion. The difference between the two temperatures of the wires, indicated as differential output temperature, is taken as the output quantity of the simulations.

4. Simulations results

The wire overheating in the TKO structure (Fig. 3a) calculated with the 3D model is shown in Fig. 5. In order to make the membrane structure visible, the air volume has been removed from the picture. It can be noted that, as expected, the maximum temperature occurs in the center of the wire while a much

smaller temperature increase is present along the two arms of the U-shaped membrane. The wire distance is 22 μm and an average wire overheating of 250 K has been obtained applying a voltage of 1.364 V across the wire.

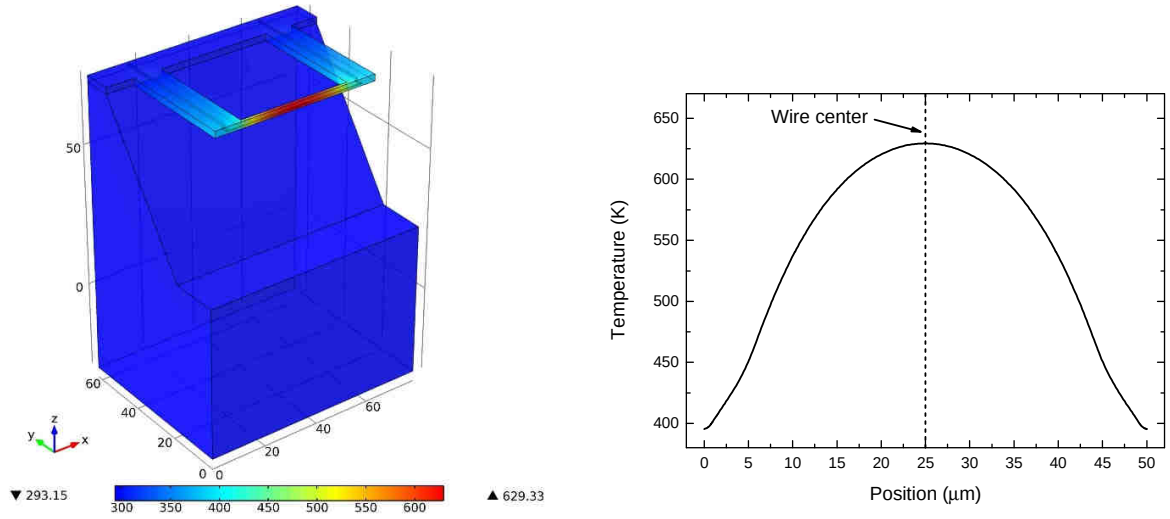

(a) (b)

Fig. 5. (a) Temperature profile of a thick oxide structure (TKO) with a wire distance of 22 μm and an applied voltage of 1.364 V; (b) temperature profile along the polysilicon wire.

The 2D simulation results have been analyzed in terms of the device sensitivity, defined as the ratio between the calculated differential output temperature and the input particle velocity, set to a constant value of 1 mm/s in all simulations.

The dependence of the sensitivity on frequency for three different values of the wire gap (d) is shown in Fig. 6 for the TKO structure (Fig. 3a).

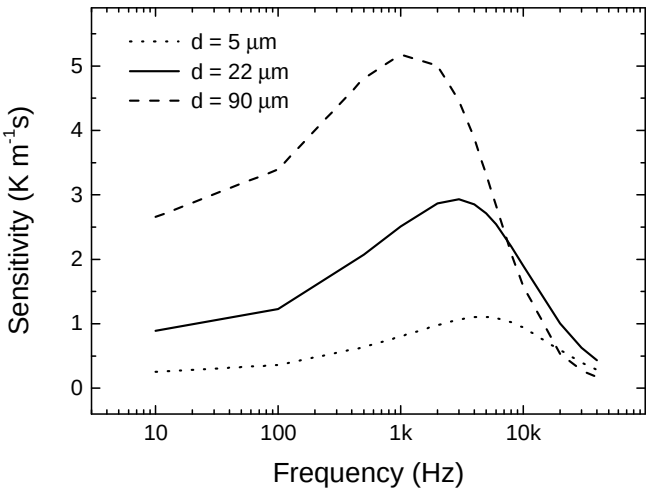

Fig. 6. Thick oxide structure (TKO) sensitivity as a function of frequency for three different values of the wire distance.

The simulations have been performed in the frequency range 10 Hz – 40 kHz. The obtained behavior is consistent with the experimental data of similar APV sensors recently proposed [15], characterized by a wire distance of 5 μm. The sensitivity decrease at low frequency can be ascribed to the boundary layer thickness dependence on frequency. In fact, the thickness of the viscous and thermal boundary layers is inversely proportional to the square root of the frequency [40]: increasing the frequency, the boundary layer thickness decreases, enhancing the heat exchange between the wires and the moving air. However, as the frequency increases, two other dynamic phenomena interfere, limiting the sensitivity increase and causing a maximum to occur and a subsequent drop at high frequency. The first phenomenon is heat transport between the two wires, which is governed by a constant time depending on the air thermal diffusivity and the wire distance [37]. The second effect is the inertia by which the wire temperature variations follow heat transfer variations. This inertia is due to the thermal mass of the polysilicon wire and of the silicon dioxide membrane. The effect of the wire distance on the frequency response can be extrapolated from the three curves shown in Fig. 6: decreasing the wire distance *d* from 90 μm to 5 μm, the sensitivity at low frequency presents a clear decrease. This effect is not easy to explain, but it can be partly ascribed to the reduction of the thermal resistance of the air gap

that separates the wires. Note that the point of maximum sensitivity shifts to higher frequencies as the air gap is reduced, making the devices with smaller air gap advantageous in the high frequency region. Nevertheless, for all curves the sensitivity in the ultrasound range (f>20 kHz) is significantly degraded for all values of the airgap *d*. The reason is the relatively high thermal mass of the TKO structure. For this reason, we expect that the other two structures in Fig. 3 (TNO and SSP) exhibit a better sensitivity at high frequency. In order to compare the three structures in the best conditions for ultrasound applications, we have first found the wire distance (*d*) that gives the best sensitivity at a frequency of 40 kHz. This has been obtained by parametric simulations where the frequency was kept fixed and the air gap was varied until a sensitivity maximum was found. Repeating this test at different frequencies, we have found the curves in Fig. 7, where the optimum distance *d* is plotted against frequency.

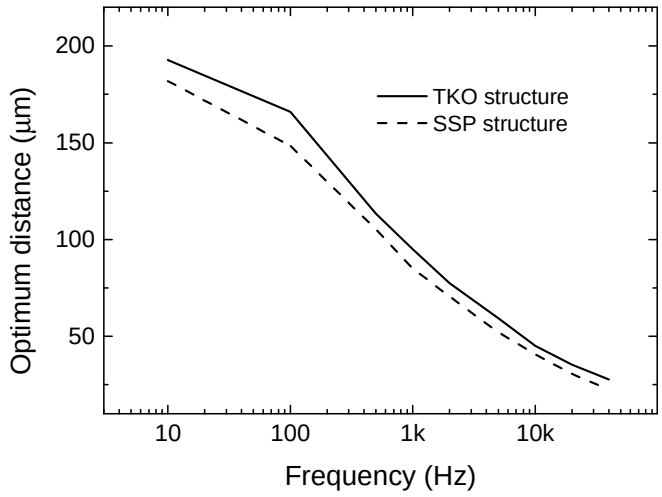

Fig. 7. Optimum wire distance as a function of frequency for the thick oxide structure (TKO) and the self-standing polysilicon structure (SSP).

The curves refer to the thick oxide and self-standing structures. It can be noted that the optimum wire distance is inversely proportional to the frequency and this behavior is valid for both type of sensors, with differences that tend to get smaller at high frequency. In particular, a SSP sensor with a wire distance of about 22 μm is the best choice for 40 kHz applications; this value is good also for a thick oxide sensor as confirmed by the data shown in Fig. 6. It should be noted that the calculated optimum

distance maximizes the response at a specific frequency, which, on the other hand, does not coincide with a frequency of maximum sensitivity. This is clearly visible in Fig. 6 where the structure with *d*=22 μm shows the maximum sensitivity at about 3 kHz.

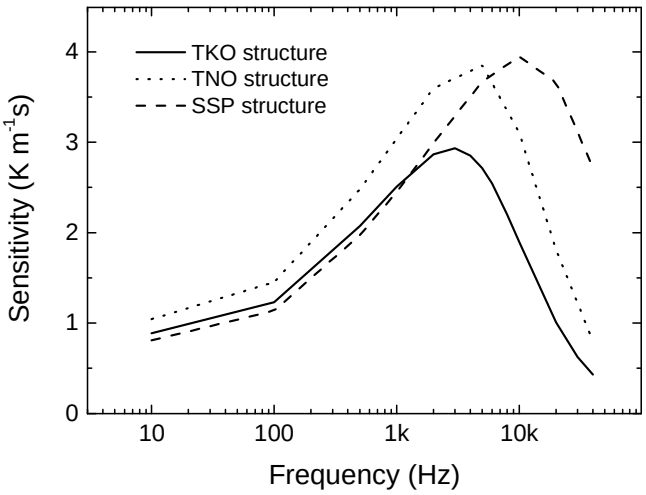

Fig. 8. Sensor sensitivity as a function of frequency for the three different structures simulated: the wire distance has been fixed at 22 μm.

Comparison of the three configurations, all designed with d=22 μm for the sake of simplicity, is presented in Fig. 8, where the frequency response is shown in all three cases. As expected, in the ultrasound region the sensitivity increases as the thermal mass is reduced. In particular, the self-standing structure presents a much higher sensitivity at 40 kHz than the other two configurations. The maximum of the sensitivity is also affected by a shift toward higher frequency when the thermal capacitance decreases and it passes from 3 kHz of the thick oxide configuration to around 10 kHz of the self-standing one.

In order to extend comparison of the three configurations over a wider frequency range, we have found the best sensitivity that can be obtained at each frequency by tuning the wire distance *d*. In practice, we have chosen a set of frequency values over the 10 Hz-40 kHz interval and, for each value, we have simulated the structure with the optimum distance for that frequency, finding the best sensitivity that can be obtained with a given configuration at that frequency. The collection of maximum sensitivities

as a function of frequency is shown in Fig. 9 for the TKO and SSP structures. This plot must be considered as the collection of the responses of structures with different wire gap, each optimized for the corresponding frequency. Thus, a single structure with the sensitivity behavior shown in the figure it does not exist, but the plot is very useful in the design phase. It is evident, for example, that at low frequency it is better to use a sensing structure with the silicon dioxide membrane while for high frequency applications the reduction of the thermal capacitance is fundamental. In fact, the maximum sensitivity at 40 kHz is S=2.4 $Km^{-1}s$ for the SSP structure obtained with d=22.5 μm and S=0.4 $Km^{-1}s$ for the TKO structure with d=28 μm. Finally, it is interesting to discuss about the maxima of the plots shown in the figure. The peak values are the best sensitivity that can be obtained with the proposed structures after the optimization of the wire distance; the peak frequency is the frequency at which the particular configuration gives the best response. In particular, the peak sensitivity of the thick oxide sensor is S = 5.1 $Km^{-1}s$ and it has been obtained at 1 kHz using d=95 μm. The peak sensitivity of the polysilicon sensor is S = 4.3 $Km^{-1}s$ and it has been obtained at 5 kHz using d=52 μm.

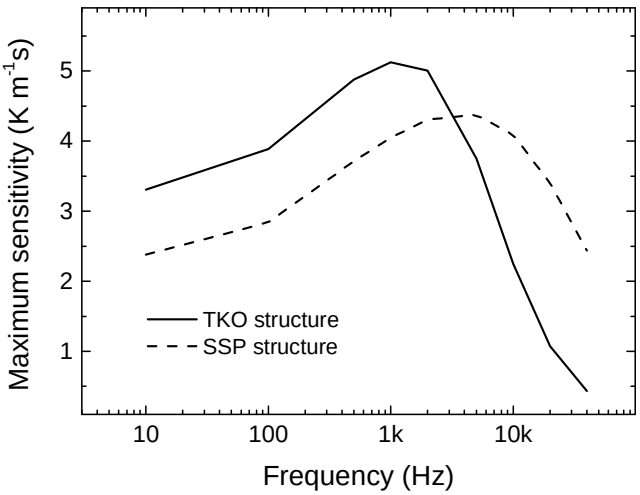

Fig. 9. Maximum of the sensitivity as a function of frequency for the thick oxide structure (TKO) and the self-standing polysilicon structure (SSP), obtained by optimizing the wire distance *d* at each individual frequency.

Just to have an idea of the electrical signal magnitude that can be produced by a sensor that exhibits the sensitivities quoted above, we can refer to a full Wheatstone bridge configuration [15] formed by two wire pairs such those depicted in Fig. 1. It can be easily shown that the output signal voltage of the bridge is given by:

$$v_{out} = \frac{\delta T \alpha V_B}{2}, \tag{2}$$

where δT is the temperature difference (between each wire pair) produced by the acoustic particle velocity, α is the wire temperature coefficient of the resistance (TCR) and V_B is the supply voltage of the bridge. Consider that $\delta T = S \cdot u$, where S is the sensitivity of the APV sensor as defined in this paper and u is the particle velocity. With V_B=10 V, $\alpha = 3\times10^{-3}$ K^{-1}, and S=2.4 $Km^{-1}s$ (maximum value achievable at 40 kHz with the SSP structure), an output voltage of 36 μV can be obtained with an APV of 1 mm/s, corresponding to a sound pressure of 86 dB (SPL). This intensity, which is generally lower than the typical sound intensity used in short distance proximity sensors, results in output signal magnitudes (tens of microvolts or higher) that can be reliably detected with a low-noise amplifiers. By these considerations, use of the SSP structure for ultrasonic application can be reasonably envisioned.

Conclusions

Three different sensing structures have been investigated by means of FEM simulations in order to explore the possibility of using APV sensors for applications in the ultrasonic frequency range. The structures consist of pairs of parallel polysilicon-silicide wires placed over suspended dielectric membranes designed with a commercial CMOS process. The main difference between the three structures is the thickness of the suspending membranes, which, for one of the examined cases, is completely removed. The results of parametric simulations confirmed the key role played by the wire distance in determining the frequency response. In particular, for all the examined structure types, we found that the distance that maximizes the sensitivity progressively decreases as the working frequency increases. The three investigated configurations show important performance differences in the

ultrasound region. In particular, we found that only the structure based on a self-standing polysilicon-silicide wire presents a sensitivity at 40 kHz that is still comparable with the sensitivities estimated in the low frequency range. Conversely, the other two structures, which suffer from the large thermal capacity of the suspending membrane, exhibit a dramatic sensitivity drop at high frequencies, which makes them practically not adequate for ultrasound applications. Fabrication of the SSP structure requires an additional process step for the removal of the whole suspending dielectric membrane. However, this issue should not be critical due to the high selectivity of silicon dioxide etchants (either in wet or vapour phase) with respect to polysilicon.

Aknowledgements

The authors would like to thank the R & D group of the STMicroelectronics of Cornaredo (MI, Italy) for providing information about the CMOS fabrication process.

Funding

Work partially supported by the Italian Ministry of Education and Research (MIUR) in the framework of the CrossLab project (Departments of Excellence).

References

[1] L. E. Kinsler, A. R. Frey, A. B. Coppens, J. V. Sanders, *Fundamentals of Acoustics, 4th Edition, by Lawrence E. Kinsler, Austin R. Frey, Alan B. Coppens, James V. Sanders,. ISBN 0-471-84789-5. Wiley-VCH, December 1999,*

[2] T. B. Gabrielson, D. L.Gardner, S. L. Garrett, A simple neutrally buoyant sensor for direct measurement of particle velocity and intensity in water, *The Journal of the Acoustical Society of America 97*(4) (1995) 2227-2237.

[3] M. Campbell, J. A. Cosgrove, C. A. Greated, S. Jack, D. Rockliff, Review of LDA and PIV applied to the measurement of sound and acoustic streaming, *Optics & laser technology*, *32*(7-8) (2000) 629-639.

[4] H. E. de Bree, P. Leussink, T. Korthorst, H. Jansen, T. Lammerink, M. Elwenspoek, (1995, June). The μ-Flown-A Novel Device Measuring Acoustical Flows, in *Proceedings of the International Solid-State Sensors and Actuators Conference-TRANSDUCERS'95* Vol. 1, (1995) 536-539.

[5] H. E. de Bree, P. Leussink, T. Korthorst, H. Jansen, T. S. Lammerink, M. Elwenspoek, The μ-flown: a novel device for measuring acoustic flows. *Sensors and actuators A: Physical 54*(1-3) (1996) 552-557.

[6] H.-E. de Bree, An overview of microflown technologies, Acta Acust. 89 (2003)163–172.

[7] Microflown Online Product Catalog. Available from: http://www.microflown.com/ (online).

[8] O. Pjetri, R. J. Wiegerink, T. S. Lammerink, G. J. Krijnen, A crossed-wire 2-dimensional acoustic particle velocity sensor, in IEEE Sensors (2013) 1-4.

[9] O. Pjetri, R. J. Wiegerink, G. J. Krijnen, A 2D particle velocity sensor with minimal flow disturbance, *IEEE sensors journal 16*(24) (2016) 8706-8714.

[10] O. Pjetri, R. J. Wiegerink, T. S. Lammerink, G. J. Krijnen, A 2D acoustic particle velocity sensor with perfectly orthogonal sensitivity directions, *Sensors and Actuators A: Physical 246* (2016) 28-34.

[11] D. R. Yntema, J. W. Van Honschoten, H. E. De Bree, R. J. Wiegerink, M. Elwenspoek, A three dimensional microflown, in *19th IEEE International Conference on Micro Electro Mechanical Systems* (2006) 654-657.

[12] D. R. Yntema, R. J. Wiegerink, J. W. Van Honschoten, M. Elwenspoek, Fully integrated three dimensional sound intensity sensor, in *2007 IEEE 20th International Conference on Micro Electro Mechanical Systems (MEMS)* (2007) 51-54.

[13] D. R. Yntema, J. W. Van Honschoten, R. J. Wiegerink, M. Elwenspoek, A complete three-dimensional sound intensity sensor integrated on a single chip, *Journal of micromechanics and microengineering*, *18*(11) (2008) 115004.

[14] P. Bruschi, F. Butti, M. Piotto, CMOS compatible acoustic particle velocity sensors, in: Proceedings of IEEE Sensors 2011, Limerick, Ireland, (2011) 1405–1408.

[15] M. Piotto, F. Butti, E. Zanetti, A. Di Pancrazio, G. Iannaccone, P. Bruschi, Characterization and modeling of CMOS-compatible acoustical particle velocity sensors for applications requiring low supply voltages. *Sensors and Actuators A: Physical*, *229* (2015) 192-202.

[16] M. Piotto, A. Ria, D. Stanzial, P. Bruschi, Design and Characterization of Acoustic Particle Velocity Sensors Fabricated with a Commercial Post-CMOS MEMS Process, in *20th International Conference on Solid-State Sensors, Actuators and Microsystems & Eurosensors XXXIII (TRANSDUCERS & EUROSENSORS XXXIII)* (2019) 1839-1842.

[17] R. Lanoye, G. Vermeir, W. Lauriks, R. Kruse, V. Mellert, Measuring the free field acoustic impedance and absorption coefficient of sound absorbing materials with a combined particle velocity-pressure sensor, *The Journal of the Acoustical Society of America*, *119*(5) (2006) 2826-2831.

[18] D. Fernandez Comesana, I. Cereijo Grana, A. Grosso, Particle velocity sensors for enhancing vehicle simulations, AIA-DAGA 2013 Merano (Italy) (2013) 1236-1239.

[19] M. Piotto, A. N. Longhitano, P. Bruschi, M. Buiat, G. Sacchi, D. Stanzial, (2014). Design and Fabrication of a Compact p–v Probe for Acoustic Impedance Measurement, in *Sensors and Microsystems* Springer (2014) 53-56.

[20] F. Jacobsen, F., H.E. de Bree, A comparison of two different sound intensity measurement principles. *The Journal of the Acoustical Society of America*, *118*(3), (2005) 1510-1517.

[21] K. N. Ramamohan, D. F. Comesaña, G. Leus, Uniaxial Acoustic Vector Sensors for direction-of-arrival estimation, *Journal of Sound and Vibration, 437* (2018) 276-291.

[22] F. Jacobsen, Y. Liu, (2005), Near field acoustic holography with particle velocity transducers, *The Journal of the Acoustical Society of America, 118*(5) (2005) 3139-3144.

[23] Z. W. Luo, D. F. Comesana, C. J. Zheng, C. X. Bi, Near-field acoustic holography with three-dimensional scanning measurements, *Journal of Sound and Vibration*, *439*, (2019) 43-55.

[24] D. F. Comesana, K. R. Holland, E. Fernandez-Grande, Spatial resolution limits for the localization of noise sources using direct sound mapping. *Journal of Sound and Vibration*, *375*, (2016) 53-62.

[25] M. Mitra, S. Gopalakrishnan, Guided wave based structural health monitoring: A review, *Smart Materials and Structures*, *25*(5) (2016) 053001.

[26] J. Moll, J. Kathol, C. P. Fritzen, M. Moix-Bonet, M. Rennoch, M. Koerdt, M. Bach, Open Guided Waves: online platform for ultrasonic guided wave measurements. *Structural Health Monitoring*, *18*(5-6), (2019) 1903-1914.

[27] T. S. Awad, H. A. Moharram, O. E. Shaltout, D. Asker, M. M. Youssef, Applications of ultrasound in analysis, processing and quality control of food: A review. *Food research international*, *48*(2), (2012) 410-427.

[28] A. Ohya, T. Ohno, Obstacle detectability of ultrasonic ranging system and sonar map understanding, *Robotics and Autonomous Systems*, *18*(1-2), (1996) 251-257.

[29] J. Park, Y. Je, H. Lee, W. Moon, Design of an ultrasonic sensor for measuring distance and detecting obstacles. *Ultrasonics*, *50*(3), (2010) 340-346.

[30] G. Gibbs, H. Jia, I. Madani, Obstacle detection with ultrasonic sensors and signal analysis metrics, *Transportation Research Procedia*, *28*, (2017) 173-182.

[31] W. Xu, C. Yan, W. Jia, X. Ji, J. Liu, Analyzing and Enhancing the Security of Ultrasonic Sensors for Autonomous Vehicles, *IEEE Internet of Things Journal*, *5*(6) (2018) 5015-5029.

[32] D. Yi, J. Joo, S. C. Kim, Implementation of DPSK-based Obstacle Detection System using UItrasound for Vehicles, in *2019 Eleventh International Conference on Ubiquitous and Future Networks (ICUFN)* (2019) 614-616.

[33] I. Ulrich, J. Borenstein, The GuideCane-applying mobile robot technologies to assist the visually impaired, *IEEE Transactions on Systems, Man, and Cybernetics, Part A: Systems and Humans*, *31*(2) (2001) 131-136.

[34] B. Mocanu, R. Tapu, T. Zaharia, When ultrasonic sensors and computer vision join forces for efficient obstacle detection and recognition. *Sensors*, *16*(11) (2016) 1807.

[35] J. Foucault, S. Lesecq, G. Dudnik, M. Correvon, R. O'Keeffe, V. Di Palma, J. Herveg, INSPEX: Optimize Range Sensors for Environment Perception as a Portable System, *Sensors*, *19*(19), (2019) 4350.

[36] A. Ria, M. Piotto, M. Cicalini, A. Nannini, P. Bruschi, 2-D Acoustic particle velocity sensors based on a commercial post-CMOS MEMS technology, Applications in Electronics Pervading Industry, Environment and Society, Lecture Notes in Electrical Engineering 627, Springer, in press.

[37] J W. van Honschoten, G. J. M. Krijnen, V. B. Svetovoy, H.-E. de Bree and M. C. Elwenspoek, Analytic model of a two-wire thermal sensor for flow and sound measurements, J. Micromech. Microeng. 14 (2004) 1468–1477.

[38] M. Piotto, F. Del Cesta, P. Bruschi, Integrated smart gas flow sensor with 2.6 mW total power consumption and 80 dB dynamic range Microelectronic Engineering 159 (2016) 159–163

[39] P. Bruschi, A. Ciomei, M. Piotto, Design and analysis of integrated flow sensors by means of a two-dimensional finite element model, Sensors and Actuators A 142 (2008) 153–159

[40] L. D. Landau, E. M. Lifshitz, Fluid mechanics, Second edition Oxford: Pergamon Press, 1987.

Authors Biographies

Lorenzo Benvenuti: Lorenzo Benvenuti was born in Empoli, Italy, in 1989. He received the M.Sc. degree in Electronics Engineering from the University of Pisa, in 2017. He is currently pursuing the Ph.D. degree at the same university, in collaboration with ScioSense, at their design center in Pisa. His main research interests include the design of integrated sensors and electronic circuits for sensor interfacing.

Alessandro Catania: Alessandro Catania was born in 1993; Pisa, Italy. He received his laurea degree in Electronic Engineering from the University of Pisa, Italy, in 2016. He is currently a Ph.D. Student in Information Engineering at Dipartimento di Ingegneria dell'Informazione of the University of Pisa. His main research interests concern integrated sensor design, analog integrated circuits for sensor interfacing and ultra-low voltage analog front-end and data converters.

Paolo Bruschi: Paolo Bruschi was born in Massa, Italy, in 1964. He received the laurea degree in Electronic Engineering from the University of Pisa, Italy, in 1989. In 1993 he joined the Department of Information Engineering as a researcher. He is currently a full professor of the Department of Information Engineering of the University of Pisa. His main area of interest is the development of integrated silicon sensors and actuators. He is also involved in the design of mixed-signal integrated circuits for sensor interfacing.

Massimo Piotto: Massimo Piotto was born in 1970, La Spezia, Italy. He received his laurea degree in Electronic Engineering from the University of Pisa, Italy, in 1996 and his Ph.D. degree in Electronic, Computer and Telecommunication Engineering in 2000. From 2001 to 2017 he was a researcher of the section of Pisa of the “Istituto di Elettronica e di Ingegneria dell’Informazione e delle Telecomunicazioni” - National Research Council. He is currently an associate professor of the Department of Information Engineering of the University of Pisa. His main research interests concern the design of integrated sensors and actuators, the development of MEMS technologies and the design of electronic circuits for sensor interfacing.

Figure Captions

Fig. 1. Schematic perspective view of a sensing structure. (not to scale)

Fig. 2. (a) Perspective and (b) plan view of a section of the sensing structure. The axis of maximum sensitivity is shown. (not to scale)

Fig. 3. Plan and cross-section views of the three different sensing structures (not to scale): (a) thick oxide structure (TKO), (b) thin oxide structure (TNO) and (c) self-standing polysilicon structure (SSP).

Fig. 4. Axonometric projection of the 3D COMSOL model used for the FEM numerical simulations

Fig. 5. (a) Temperature profile of a thick oxide structure (TKO) with a wire distance of 22 μm and an applied voltage of 1.364 V; (b) temperature profile along the polysilicon wire.

Fig. 6. Thick oxide structure (TKO) sensitivity as a function of frequency for three different values of the wire distance.

Fig. 7. Optimum wire distance as a function of frequency for the thick oxide structure (TKO) and the self-standing polysilicon structure (SSP).

Fig. 8. Sensor sensitivity as a function of frequency for the three different structures simulated: the wire distance has been fixed at 22 μm.

Fig. 9. Maximum of the sensitivity as a function of frequency for the thick oxide structure (TKO) and the self-standing polysilicon structure (SSP), obtained by optimizing the wire distance *d* at each individual frequency.

FIGURES

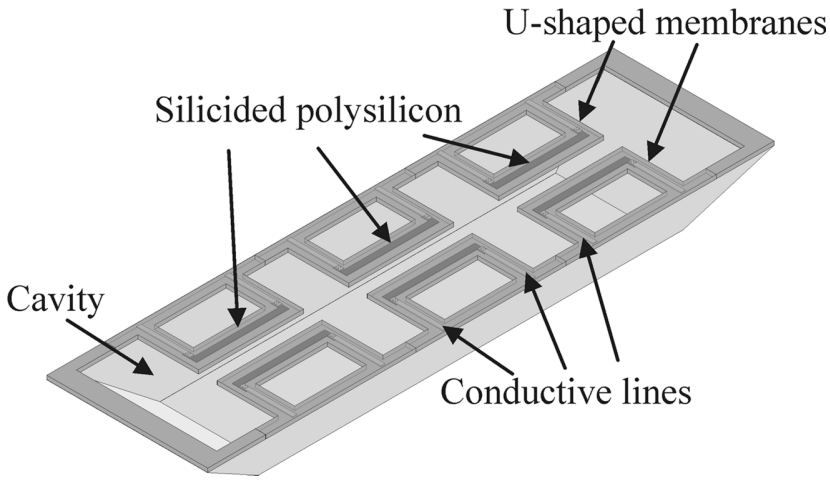

Figure 1

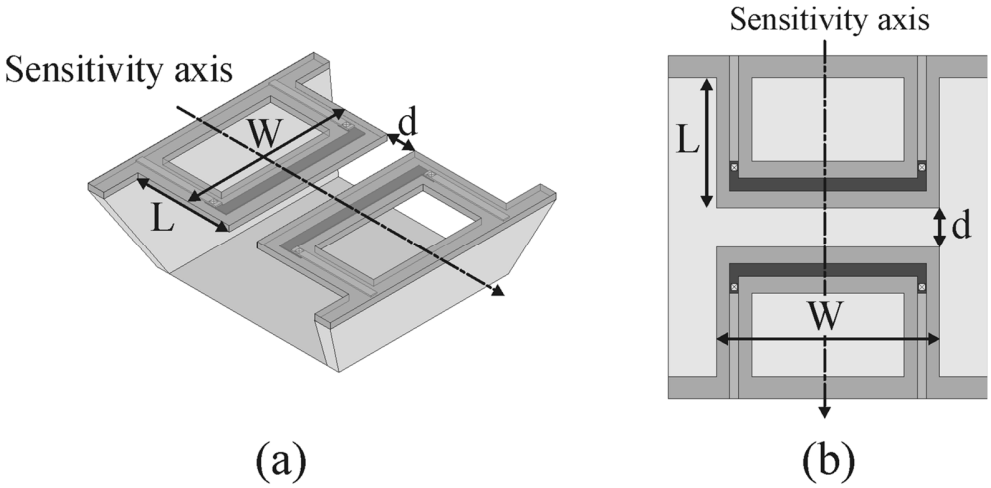

Figure 2

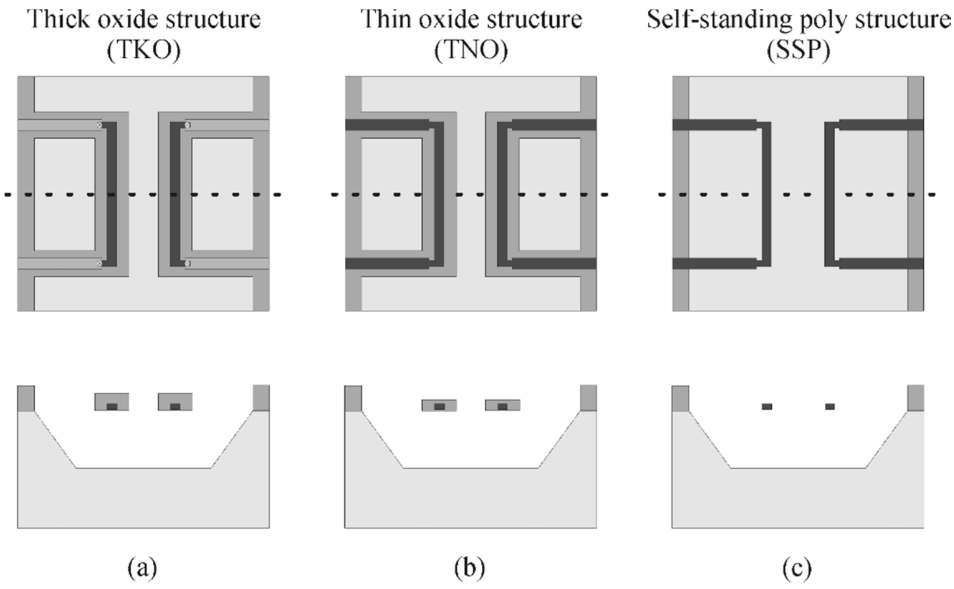

Figure 3

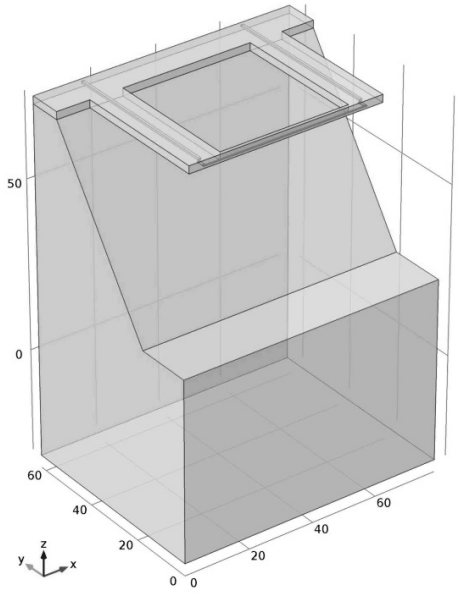

Figure 4

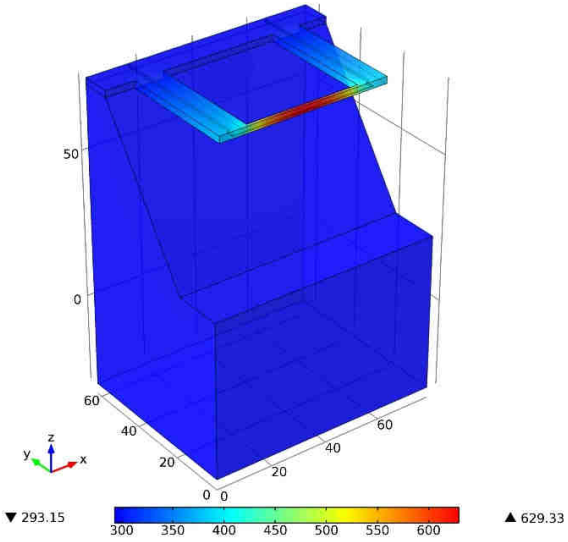

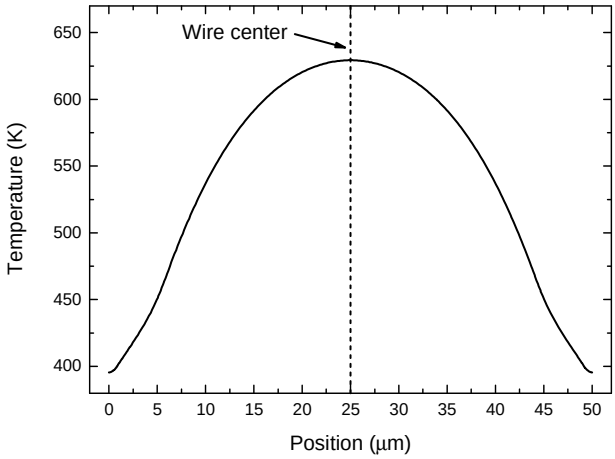

(a) (b)

Figure 5

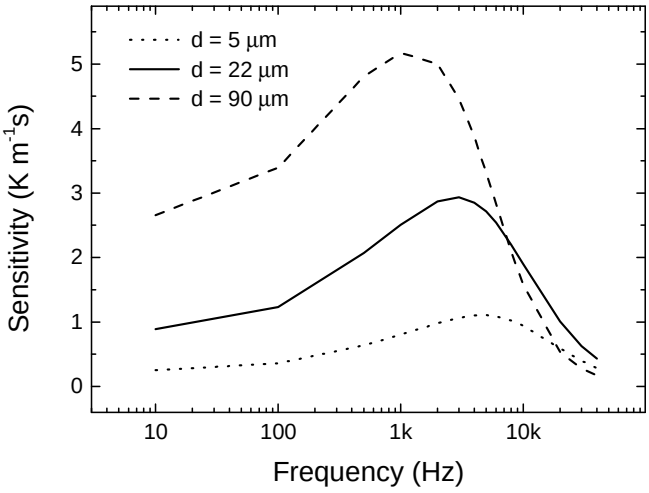

Figure 6

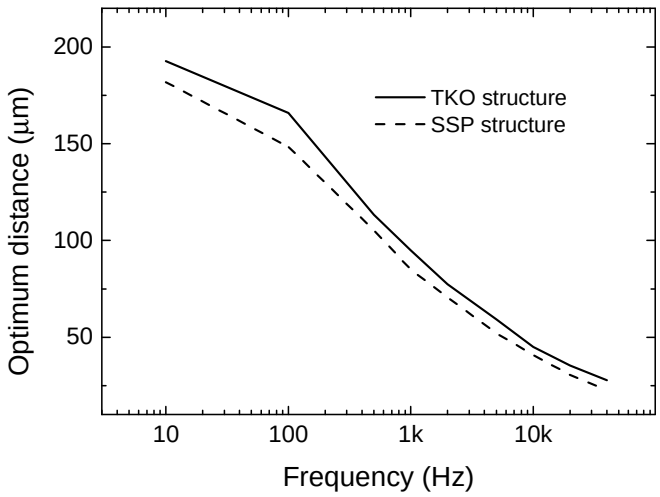

Figure 7

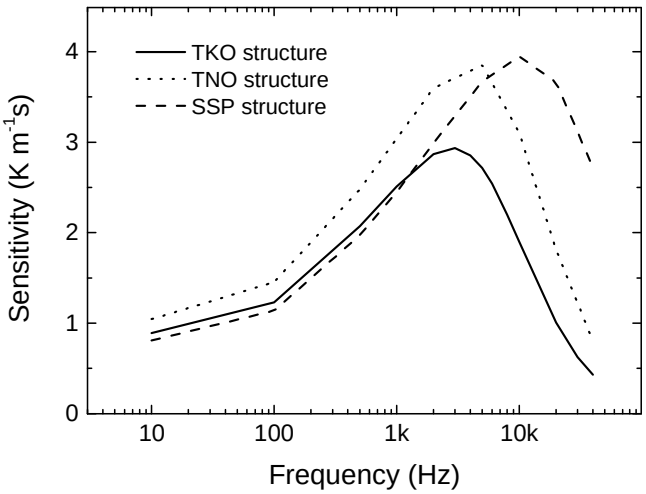

Figure 8

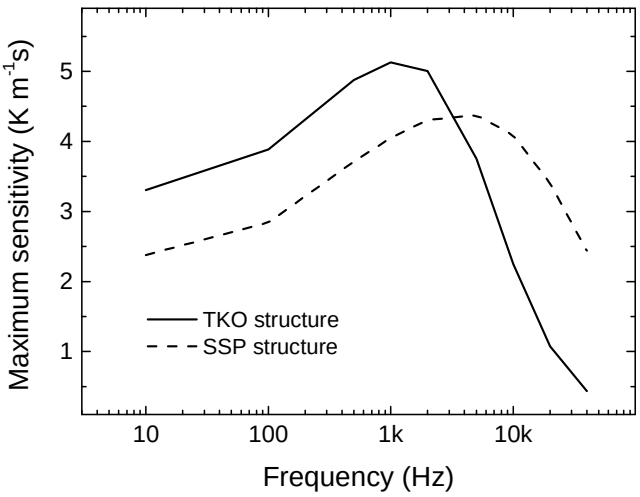
Maximum sensitivity (K m-1s)
5
4
3
2
1
10
100
1k
10k
Frequency (Hz)
TKO structure
SSP structure

Figure 9